

Crossing the Human-Robot Embodiment Gap with Sim-to-Real RL using One Human Demonstration

Tyler Ga Wei Lum* Olivia Y. Lee* C. Karen Liu Jeannette Bohg

Stanford University

<https://human2sim2robot.github.io/>

Abstract—Teaching robots dexterous manipulation skills often requires collecting hundreds of demonstrations using wearables or teleoperation, a process that is challenging to scale. Videos of human-object interactions are easier to collect and scale, but leveraging them directly for robot learning is difficult due to the lack of explicit action labels from videos and morphological differences between robot and human hands. We propose HUMAN2SIM2ROBOT, a novel real-to-sim-to-real framework for training dexterous manipulation policies using only one RGB-D video of a human demonstrating a task. Our method utilizes reinforcement learning (RL) in simulation to cross the human-robot embodiment gap without relying on wearables, teleoperation, or large-scale data collection typically necessary for imitation learning methods. From the demonstration, we extract two task-specific components: (1) the object pose trajectory to define an object-centric, embodiment-agnostic reward function, and (2) the pre-manipulation hand pose to initialize and guide exploration during RL training. We found that these two components are highly effective for learning the desired task, eliminating the need for task-specific reward shaping and tuning. We demonstrate that HUMAN2SIM2ROBOT outperforms object-aware open-loop trajectory replay by 55% and imitation learning with data augmentation by 68% across grasping, non-prehensile manipulation, and multi-step tasks. Project Site: human2sim2robot.github.io

I. INTRODUCTION

Training robotic manipulation policies from demonstrations via imitation learning (IL) has gathered considerable interest [1, 2, 12, 19, 23]. A key requirement for effective IL is the availability of high-quality demonstrations composed of sequences of states with corresponding robot action labels. This is typically acquired through labor-intensive data collection requiring hundreds or thousands of human demonstrations per task via teleoperation or specialized wearable equipment [10, 28, 53]. In contrast, videos of humans interacting with objects with their own hands are inexpensive to collect, a scalable alternative to traditional demonstration collection methods. However, leveraging human videos directly for IL is challenging as they lack explicit robot action labels [57].

One popular approach to address this is by obtaining per-timestep human hand pose estimates and converting them to robot action labels via fingertip retargeting and inverse kinematics (IK) [4, 53]. However, this approach faces two challenges. First, while recent hand pose reconstruction methods have shown impressive performance [38], their predictions are still not always accurate due to occlusions and sensor noise, resulting in mismatches between the robot hand IK targets and the true human hand fingertips. Second, even with perfect

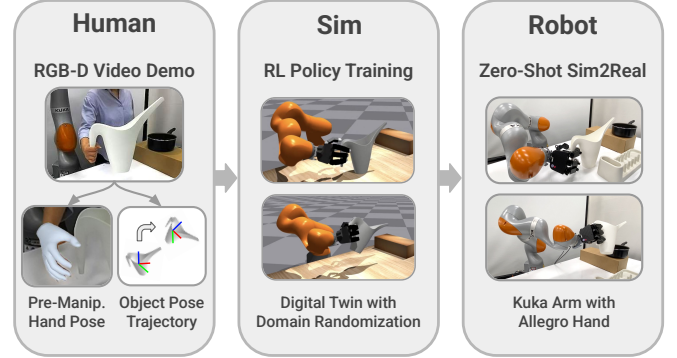


Fig. 1. **Our Framework.** HUMAN2SIM2ROBOT is a real-to-sim-to-real RL framework for learning dexterous manipulation policies from one human RGB-D video demonstration per task. From the demonstration, we leverage object pose trajectories and pre-manipulation hand poses to provide guidance and advantageous initialization for RL training in simulation. These policies demonstrate zero-shot sim-to-real transfer to a Kuka arm and Allegro hand.

human hand pose estimates, the considerable embodiment gap between human and robot hands may make solving IK infeasible or result in suboptimal robot joint configurations for the demonstrated task. Both challenges are particularly punishing for contact-rich, dexterous manipulation tasks using multi-fingered robotic hands as they require precise coordination of forces and motion at multiple contact points, which is difficult to achieve when retargeted actions are noisy or suboptimal for the target embodiment [3, 32, 37]. Existing IL methods are ill-equipped to address this issue as they rely on accurate correspondences between the demonstrated and learned behaviors. Reinforcement learning (RL) offers a promising alternative to overcome these limitations by enabling the robot to directly learn manipulation tasks using its own embodiment. However, RL has several limitations such as tedious, task-specific reward engineering and unfavorable sample complexity, which make training real-world policies infeasible [49, 60].

We propose HUMAN2SIM2ROBOT, a real-to-sim-to-real RL framework that addresses these limitations by learning robust dexterous manipulation policies from a single human hand RGB-D video demonstration. We extract two task-specific components from the video: (1) the object 6D pose trajectory, which defines an object-centric reward function that specifies the desired task while accommodating embodiment differences, and (2) the pre-manipulation hand pose, which provides advantageous initialization of RL training such that the resulting policy converges on a similar manipulation strategy shown in the demonstration. Formalizing an expert task demonstration with these two components facilitates RL policy

*Equal contribution. Please direct all correspondence to: {tylerlum, oliviayl}@stanford.edu

training with no task-specific reward tuning. Instead of directly learning state-action mappings, we use the demonstration for *task specification* and *guidance*, encouraging human-like behavior when beneficial while allowing deviations when the human strategy is unsuitable for the robot’s embodiment. HUMAN2SIM2ROBOT policies achieve zero-shot sim-to-real transfer on a real dexterous robot, without requiring wearable technologies, teleoperation, or large-scale data collection.

To the best of our knowledge, HUMAN2SIM2ROBOT is the first system that learns a robust real-world dexterous manipulation policy from only one human RGB-D video demonstration, bridging the human-robot embodiment gap for a wide range of grasping, non-prehensile manipulation, and multi-step tasks. Our extensive ablation studies demonstrate the importance of our system’s design decisions. While individual components have precedents, these works are often limited to simulation [42, 47], are not reactive closed-loop policies [6, 22, 56], require significantly more demonstrations [25, 42, 47, 58], or only perform prehensile manipulation [42, 47, 56, 22]. We demonstrate that HUMAN2SIM2ROBOT is highly effective for training task-specific RL policies in simulation. The resulting policies can execute diverse real-world dexterous manipulation tasks, such as pouring from a pitcher, pivoting a box against a wall, inserting a plate into a dishrack, or even composed sequences of tasks, without any task-specific reward tuning. In the challenging single demonstration regime, HUMAN2SIM2ROBOT outperforms object-aware open-loop trajectory replay by 55% and imitation learning with data augmentation by 68% across grasping, non-prehensile and extrinsic manipulation, and complex multi-step tasks.

II. RELATED WORK

A. Imitation Learning for Robotics

1) *Visuomotor Imitation Learning*: Recent work in visuomotor IL for robotic manipulation has shown success learning from a large number of expert demonstrations [1, 2, 9, 19, 23, 28, 53, 59]. Demonstrations are typically collected through teleoperation or specialized wearable equipment [10, 28, 53] like motion capture gloves, AR/VR equipment, or portable robot hands, which makes scaling of data collection efforts expensive. In contrast, videos of human demonstrations are inexpensive to collect and more intuitive to demonstrators. Since videos lack explicit action labels, a popular approach is to obtain per-timestep human hand pose estimates and convert them into robot action labels through IK-based retargeting [4, 53]. However, the human-robot embodiment gap often makes finding an IK solution infeasible or result in a robot joint configuration that is suboptimal for reproducing the demonstrated task. This poses significant challenges for visuomotor IL methods that directly rely on accurate correspondences between the demonstrated and learned behaviors.

Therefore, instead of directly learning a mapping from observations to actions, HUMAN2SIM2ROBOT performs RL in simulation guided by a single human video demonstration. This approach acknowledges that while human demonstrations provide useful guiding strategies for completing the task, certain actions may not be suitable for robots given substantial embodiment differences. Learning dexterous manipulation

policies with RL hence encourages human-like behavior when beneficial while allowing deviations when the human strategy is unsuitable for the robot’s embodiment. Furthermore, robust recovery and retry behavior emerges as a result of training and does not need to be explicitly demonstrated as in IL.

2) *One-Shot & Few-Shot Imitation Learning*: Another category of IL methods that parallels our approach follows the one-shot IL (OSIL) paradigm, where a single demonstration is provided. Past work has performed object pose estimation [18, 51] or object-aware retargeting using open-world vision models [27] to transfer the demonstrated trajectory to novel scenes, or adapted the single demonstration to a new scene by leveraging object segmentation and visual servoing to move the robot’s end effector to the same position relative to the object before replaying the demonstration [50]. Beyond strictly using one demonstration, a related approach collects a small number (~ 5) of teleoperated demonstrations per task, then generates more data by retargeting demonstrations to new initial conditions and rolling out these trajectories in a simulated digital twin, executing these actions in the real world if they successfully complete the task in simulation [20].

While these approaches are more data-efficient than visuomotor IL policies, they suffer from limited generalization beyond the demonstrated actions. Furthermore, when learning from human video demonstrations, object and hand pose estimates are often inaccurate due to occlusions and noise. Even if pose estimates are accurate, the human-robot embodiment gap causes IK-based retargeting to produce infeasible robot hand trajectories. Therefore, simply replaying modified versions of the single demonstration or directly learning observation-to-action mappings from retargeted data is unlikely to succeed. Our insight is that using the single human video demonstration to provide task specification and guidance for RL more effectively leverages this data source for robot learning. This allows robots to develop effective strategies with their own embodiment, rather than rigidly imitating human behaviors.

B. Reinforcement Learning for Robotics

Reinforcement learning (RL) is a method for training autonomous agents to perform complex tasks by interacting with an environment through trial and error. In this work, we train manipulation policies in simulation to avoid the pitfalls of RL in the real world such as slow training, unsafe behavior, frequent environment resets and difficult to tune reward functions [49, 60]. Sim-to-real RL has shown significant promise across a wide range of robotic tasks, achieving state-of-the-art performance in domains such as legged locomotion [7, 35, 36], drone racing [21], bipedal soccer [17], and in-hand manipulation [41]. However, this potential has yet to be fully realized for dexterous manipulation over the full robot arm-and-hand kinematics: many prior works on RL for dexterous manipulation are confined to simulation with non-physical, floating-hand robots [5, 43, 52, 55].

Recent works leveraging sim-to-real RL for real-world manipulation tasks have used RL to fine-tune a BC policy [49] or learn a residual policy that outputs delta actions relative to an open-loop base motion [6]. Fine-tuning a BC policy may learn

more stably, but requires a demonstration dataset with the same robot embodiment. Residual policy learning can be effective, but only allows small adjustments to the base motion, limiting its ability to overcome large embodiment gaps or demonstrate retry behavior. Additionally, both methods require accurate human action sequences from high-quality motion capture or teleoperation. HUMAN2SIM2ROBOT is a real-to-sim-to-real framework that trains an RL policy over a full arm-and-hand action space, guided by object-centric rewards and a pre-manipulation hand pose from just one human demonstration. This approach can thus accommodate lower-quality human video demonstration data, facilitate learning of retry behavior, and overcome the human-robot embodiment gap. Furthermore, our approach enables policies to learn contact-rich dexterous manipulation tasks that are more complex than parallel-jaw pick-and-place or in-hand manipulation with a static arm.

Lum et al. [30] trains dexterous grasping policies using sim-to-real RL with a geometric fabric controller, enabling smooth, coordinated motion while effectively avoiding undesired collisions with the environment. However, the policy is limited to a simple grasping task, typically converging on a simple top-down grasp as the hand is initialized above the object and the policy is trained from scratch without human guidance. HUMAN2SIM2ROBOT leverages a similar geometric fabric controller, but enables policies to perform more general prehensile and non-prehensile manipulation tasks by incorporating human guidance on how to perform the task.

Recent studies corroborate the observation that pre-grasp hand configurations can accelerate policy learning and result in human-like grasps [11, 14, 31]. These methods only focus on grasping tasks, use pre-grasps from very similar embodiments, and have only been tested in simulation. In this work, we focus on training RL policies that transfer to the real-world, overcome the human-robot embodiment gap, and perform both prehensile and non-prehensile manipulation. Furthermore, we incorporate scalable methods for pre-manipulation hand pose acquisition from one human video demonstration.

Another line of work uses inverse RL on human videos [25, 58], but inferring a reward function typically requires ~ 100 demos. In contrast, our explicit object-centric reward is designed for sample efficiency in the single-demo regime.

III. METHOD

We present HUMAN2SIM2ROBOT, a real-to-sim-to-real RL framework for learning robust, dexterous manipulation policies from a single human-hand RGB-D video demonstration. Figure 1 shows an overview of our framework. The following sections detail key design decisions of our framework.

A. Real-to-Sim & Human Demonstration

We first create a digital twin of the robot’s real-world environment and the target object to act as a policy training ground in simulation. Concretely, we use off-the-shelf 3D LiDAR scanning apps, Kiri Engine [24] and 3D Scanner App [26], to capture a high-fidelity object mesh \mathcal{O} and scene mesh \mathcal{S} , respectively, with a few minutes of human effort.

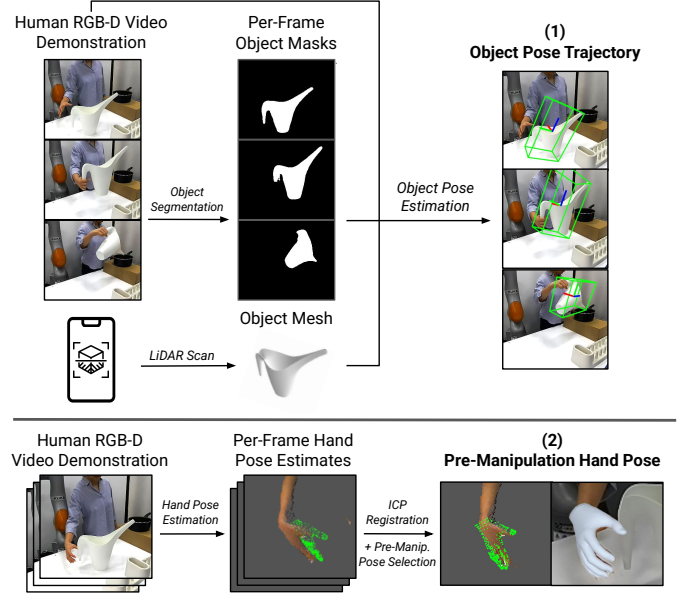


Fig. 2. **Human Demonstration Processing.** We extract two task-specific components from the human hand RGB-D video demonstration: (1) the object pose trajectory, which defines an object-centric, embodiment-agnostic reward function, and (2) the pre-manipulation hand pose, which provides advantageous initialization for RL policy training. We use FoundationPose [54] for object pose estimation (requires per-frame object masks obtained via SAM 2 [44] and object mesh [24]) and HaMeR [38] for hand pose estimation.

Next, we use a camera with known intrinsic and extrinsic parameters to record a single monocular RGB-D video demonstration $\{\mathbf{I}_t\}_{t=1}^T$, where $\mathbf{I}_t \in \mathbb{R}^{H \times W \times 4}$ is the RGB-D image at timestep $t \in \mathbb{N}$, $T \in \mathbb{N}$ is the total number of timesteps, and H and W are the image height and width, respectively.

Figure 2 visualizes how we process the human demonstration to obtain (1) an object pose goal trajectory $\{\mathbf{T}_t^{\text{goal}}\}_{t=1}^T$, and (2) a human hand pose trajectory represented as MANO [45] parameters $\{(\theta_t, \beta_t)\}_{t=1}^T$. At each timestep t , $\mathbf{T}_t^{\text{goal}} \in \text{SE}(3)$ is the object pose from the demonstration’s object trajectory, $\theta_t \in \mathbb{R}^{48}$ is the MANO hand pose parameter, and $\beta_t \in \mathbb{R}^{10}$ is the MANO hand shape parameter. In our system, we extract the object pose trajectory using FoundationPose [54], an open-source object pose detection model, which requires the scanned object mesh \mathcal{O} and per-timestep object masks generated using Segment Anything Model 2 (SAM 2) [44], an open-source segmentation model. We extract per-timestep human hand poses using HaMeR [38], an open-source hand pose detection model. Since HaMeR takes RGB images as input, we use accurate depth values from depth images and perform ICP registration to align the hand point clouds for obtaining accurate hand poses (see Appendix A for details).

Next, we determine the pre-manipulation hand pose at timestep $\tau = t_0 - t_{\text{offset}}$, where we define t_0 as the first timestep in which the object’s velocity exceeds a threshold $v_{\text{min}} = 5\text{cm/s}$, and $t_{\text{offset}} = 10$ represents a fixed number of timesteps prior to the object’s motion. We then use θ_τ and β_τ to compute the fingertip positions and the middle finger base knuckle pose as the human pre-manipulation hand pose.

Lastly, we retarget the human pre-manipulation hand pose to a robot hand pose through a two-step IK procedure using cuRobo [48]. Figure 3 visualizes how we perform human-to-

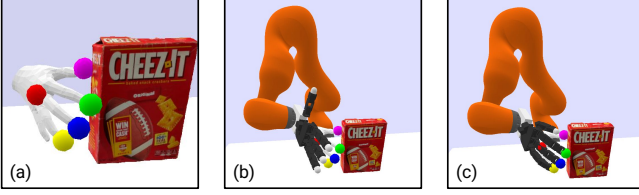


Fig. 3. **Human to Robot Hand Retargeting.** (a) MANO hand pose estimated by HaMeR [38] and aligned using ICP registration. Colored spheres denote IK retargeting points on the human hand: middle knuckle (red) and fingertips (pink, green, blue, yellow). (b) IK Step 1 (Arm): Robot hand’s middle finger base is aligned with the human hand’s middle finger knuckle. (c) IK Step 2 (Hand): Fingertips of human and robot hands are aligned.

robot hand retargeting. In the first step, the robot arm’s joint angles are adjusted to align the base position and orientation of the robot hand’s middle knuckle with that of the human hand (with a small offset, see Appendix B for details). In the second step, the robot hand’s joint angles are adjusted to align the robot’s fingertip positions with the corresponding human fingertip positions. This generates a pre-manipulation robot hand pose ($\mathbf{T}_\tau^{\text{goal}}, \mathbf{q}^{\text{hand}}$) for the object pose represented as $\mathbf{T}_\tau^{\text{goal}}$, where $\mathbf{T}_\tau^{\text{wrist}} \in \text{SE}(3)$ is the robot wrist pose, and $\mathbf{q}^{\text{hand}} \in \mathbb{R}^{N_{\text{hand-joints}}}$ is robot hand joint configuration. $N_{\text{hand-joints}} = 16$ for the Allegro hand. This simple IK process faithfully retargets the human pre-manipulation hand pose, while maintaining kinematic feasibility and alignment between human and robot hand configurations.

The object pose trajectory is used for *task specification* by defining an object-centric trajectory-tracking reward function used for policy training. The human pre-manipulation hand pose is used for *task guidance* by defining a good reset state initialization for exploring how to perform the task [14]. We note that the pre-manipulation hand pose retargeting process does not need to be extremely precise, as it is only used as a prior from which to explore and improve from. Together, these abstractions jointly guide RL policy training in simulation via reward guidance and advantageous state initializations.

B. Simulation-based Policy Learning

We create a training environment in the IsaacGym simulator [34] that matches the real-world environment, consisting of the dexterous robot, the scene mesh \mathcal{S} , and the object mesh \mathcal{O} . We then train a policy using Proximal Policy Optimization [46] which outputs robot actions that move the object along the desired goal trajectory, guided by the provided pre-manipulation hand pose. We emphasize that we primarily care about *how the object moves*, rather than imitating the actions of the human demonstration; the pre-manipulation hand pose serves as a rough prior, but the policy will learn to use the robot embodiment to achieve the desired object motion.

The reward given at timestep t is a simple object-tracking reward, $r_t = r_t^{\text{obj}}$, defined as

$$r_t^{\text{obj}} = \exp(-\alpha d(\mathbf{T}_{\tau+t}^{\text{goal}}, \mathbf{T}_t^{\text{obj}})) \quad (1)$$

We define the relative pose distance function, d , as

$$d(\mathbf{T}_1, \mathbf{T}_2) = \sum_{i=1}^{N_{\text{anchor}}} \|\mathbf{T}_1 \mathbf{k}_i - \mathbf{T}_2 \mathbf{k}_i\| \quad (2)$$

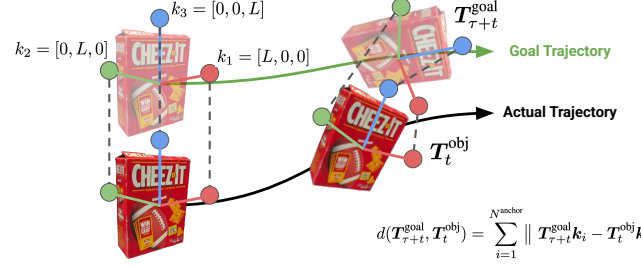


Fig. 4. **Object Pose Tracking Reward.** The agent is rewarded for moving the object along a goal trajectory by minimizing relative pose distance $d(\mathbf{T}_{\tau+t}^{\text{goal}}, \mathbf{T}_t^{\text{obj}})$, computed using anchor points $\{\mathbf{k}_i\}_{i=1}^{N_{\text{anchor}}}$ in the local frame, where L is a distance parameter for orientation. For the goal trajectory, the $t = \tau$ offset accounts for the start of the demonstration when the object is stationary, which is removed from the goal trajectory for reward computation.

For most objects, we select $N_{\text{anchor}} = 3$, with $\mathbf{k}_1 = [L, 0, 0]$, $\mathbf{k}_2 = [0, L, 0]$, and $\mathbf{k}_3 = [0, 0, L]$ in the local object frame, where L is a distance parameter for orientation. Figure 4 visualizes the object pose trajectory tracking reward. This formulation integrates both position and orientation in a physically interpretable manner: larger values of L increase the influence of orientation, since the anchor points lie farther from the object’s origin. Moreover, it is flexible enough to handle rotational symmetries or axis invariances by removing or repositioning anchor points as needed (see Appendix C for details on modifying anchor points for a rotationally symmetric object). Apart from the adjustments for rotationally symmetric objects, we use the same value for hyperparameter L for all tasks in the experiments. This highlights the generality and robustness of the proposed reward specification, making it broadly applicable across various tasks and objects.

The observation at timestep t , \mathbf{o}_t is defined as

$$\mathbf{o}_t = [\mathbf{q}_t, \dot{\mathbf{q}}_t, \mathbf{X}_t^{\text{fingertips}}, \mathbf{x}_t^{\text{palm}}, \mathbf{X}_t^{\text{obj}}, \mathbf{X}_{\tau+t}^{\text{goal}}] \quad (3)$$

where $\mathbf{q}_t \in \mathbb{R}^{N_{\text{joints}}}$ is the vector of robot joint angles, $\dot{\mathbf{q}}_t \in \mathbb{R}^{N_{\text{joints}}}$ is the vector of robot joint velocities, $\mathbf{X}_t^{\text{fingertips}} \in \mathbb{R}^{N_{\text{fingers}} \times 3}$ contains 3D positions of each fingertip, $\mathbf{x}_t^{\text{palm}} \in \mathbb{R}^3$ is the palm center’s 3D position, and $\mathbf{X}_t^{\text{obj}}, \mathbf{X}_{\tau+t}^{\text{goal}} \in \mathbb{R}^{N_{\text{anchor}} \times 3}$ contain 3D positions of the anchor points representing the current and goal object pose, respectively. $N_{\text{joints}}, N_{\text{fingers}} \in \mathbb{N}$ are the number of robot joints and fingers, respectively.

The action at timestep t , \mathbf{a}_t , is defined as

$$\mathbf{a}_t = [\mathbf{x}_t^{\text{palm-target}}, \mathbf{r}_t^{\text{palm-target}}, \mathbf{x}_t^{\text{pca-target}}] \quad (4)$$

where $\mathbf{x}_t^{\text{palm-target}} \in \mathbb{R}^3$ is the target palm center position, $\mathbf{r}_t^{\text{palm-target}} \in \mathbb{R}^3$ represents the target palm orientation expressed as Euler angles, and $\mathbf{x}_t^{\text{pca-target}} \in \mathbb{R}^{N_{\text{pca}}}$ represents the target PCA values used to control the hand configuration, where $N_{\text{pca}} = 5$ is the number of principal components. We employ a geometric fabric controller and action space similar to the approach introduced in Lum et al. [30]. In this framework, hand configurations are controlled via a lower-dimensional PCA representation, enabling human-like grasping and manipulation. For more details on this action space formulation and its benefits, we refer readers to their work.

We use an initial state distribution, guided by the human pre-manipulation hand pose, to simplify exploration and bias the

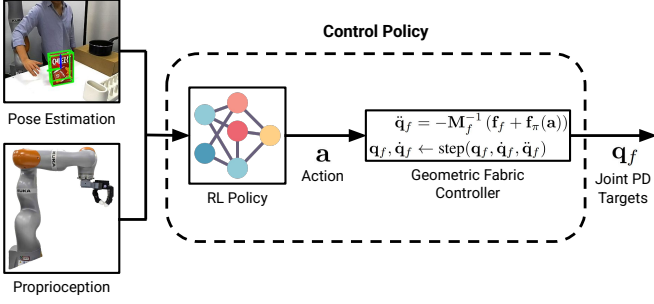


Fig. 5. **Inference-Time Diagram.** The RL policy takes object pose and robot proprioception as input. It outputs an action that is sent to a geometric fabric controller [30], which generates joint PD targets. See more at Appendix D.

policy toward learning human-like behavior. We construct this distribution by sampling the object pose around the trajectory’s initial object pose, then set the robot configuration to match the pre-manipulation hand pose with slight perturbation (see Appendix E for details). Given this perturbed hand pose, we compute a feasible arm joint angle configuration with IK¹. The environment is reset if the object is too far from the goal $d(\mathbf{T}_{\tau+t}^{\text{goal}}, \mathbf{T}_t^{\text{obj}}) > D_{\max}$, the robot palm is too far from the object $\|\mathbf{x}_t^{\text{palm}} - \mathbf{x}_t^{\text{obj}}\| > D_{\max}$, or the total timesteps of the goal trajectory is reached $\tau + t > T$, where $D_{\max} = 0.25m$.

When capturing the real-world scene, the exact dynamics parameters (e.g., the object’s mass, inertia, and friction, the friction properties of the table and robot hand) are often unknown. To address this uncertainty, we employ domain randomization during simulation training, enabling the resultant policy to perform adaptively in a diverse range of dynamic environmental conditions and facilitating sim-to-real transfer.

We train an LSTM-based policy capable of leveraging a history of observations to extract temporal information and address challenges such as noisy or incomplete data, hidden states, and partial observability. By incorporating sequential context, the policy can intelligently handle scenarios involving noisy object poses, unknown system dynamics parameters, and other sources of uncertainty to produce more effective actions. We train the policy with object pose instead of image observations, speeding up training due to the low-dimensional observation space and the absence of image rendering, while also enabling robustness to visual changes and distractors. We also train the policy with object pose observation noise to improve its robustness to pose prediction errors and camera calibration errors. Additionally, we introduce object perturbations using random forces. This, together with extensive domain randomization, improves the policy’s ability to policy handle unexpected contacts, physical disturbances, and variations in dynamic parameters, resulting in robust zero-shot sim-to-real policy transfer. See Appendix F for more training details.

C. Sim-to-Real

After training, we deploy the policy on a real robot without additional fine-tuning (i.e., zero-shot). Figure 5 illustrates the

¹We use cuRobo [48] to perform parallelized, collision-free IK to ensure RL training performance is not bottlenecked by IK computations

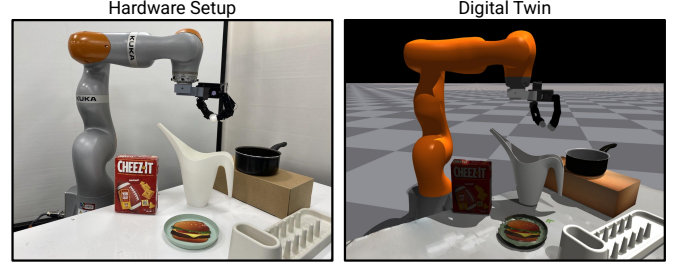


Fig. 6. **Hardware Setup & Digital Twin.** The hardware setup includes an Allegro hand mounted on a KUKA LBR iiwa 14 arm with a ZED 1 stereo camera mounted on the table (images from the camera’s perspective). Experiments are conducted in a tabletop setting with a static box, saucepan, and dishrack, involving manipulation tasks with three objects: snackbox, pitcher, and plate. The right image illustrates our digital twin.

control pipeline at deployment, highlighting the inputs and outputs of our policy at test time. We track object 6D poses at 30Hz using FoundationPose [54]. The RL policy processes real-time observations and outputs actions at 15Hz, which are then passed to a geometric fabric controller [30] running at 60Hz. Finally, this controller produces robot joint PD targets, which are executed by a low-level PD controller at 200Hz.

IV. EXPERIMENTS & RESULTS

Our experiments aim to answer the following questions:

- 1) **Importance of Embodiment-Specific RL:** Do RL policies trained via HUMAN2SIM2ROBOT outperform baselines on dexterous manipulation tasks?
- 2) **Importance of Object Pose Trajectory:** How effective is the object pose trajectory from a human demonstration as a dense reward for RL policy training, compared to other reward formulations?
- 3) **Importance of Pre-Manipulation Pose Initialization:** Does a pre-manipulation hand pose from a human demonstration provide more effective initialization for learning manipulation skills than generic initializations?
- 4) **Sufficiency of Pre-Manipulation Hand Pose:** How effective is a single pre-manipulation pose in guiding RL policy training, compared to alternatives that require full human hand trajectories?

We evaluate HUMAN2SIM2ROBOT in simulation and on a real robot across a diverse set of tasks and objects to answer these questions, which we describe in more detail below.

A. Experimental Setup

Hardware Setup. Figure 6 shows our real-world hardware setup and objects, as well as our corresponding digital twin in simulation. Our robot consists of a 16-DoF dexterous Allegro hand mounted on a 7-DoF KUKA LBR iiwa 14 arm. We use a ZED 1 stereo camera mounted to the table for both recording the human demonstration and real-time object pose estimation for policy input at test time. Our experiments are conducted in a tabletop setting with three static objects on the table: a box, a large saucepan placed atop the box, and a dishrack. The tabletop and its static objects are captured in scene scan \mathcal{S} .

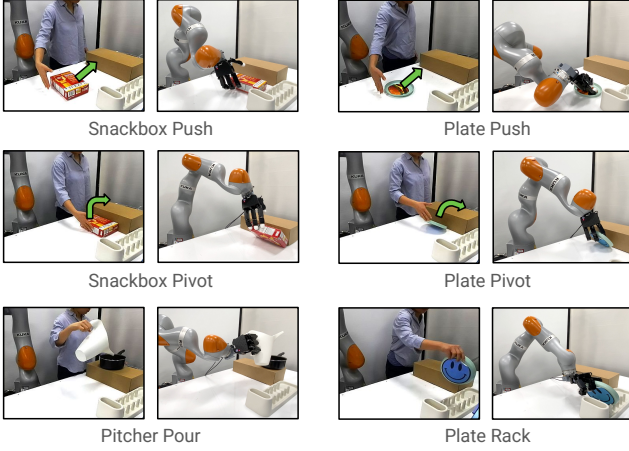


Fig. 7. **Task Visualization.** We visualize our real-world tasks spanning grasping, non-prehensile manipulation, and extrinsic manipulation, with the human demonstration and corresponding real robot behavior. We also have 3 complex multi-step tasks composing multiple skill types shown above: snackbox push-pivot, plate lift-rack, plate pivot-lift-rack.

Tasks & Objects. We perform experiments with three objects: `snackbox`, `pitcher`, and `plate`. Figure 7 visualizes our tasks using these objects, which include grasping, non-prehensile manipulation, and extrinsic manipulation. We also explore multi-step tasks that compose sequences of these skills, such as pivoting the plate, lifting it, and then placing it in a dishrack (see Appendix G for the full task list).

B. Importance of Embodiment-Specific RL

To highlight the benefits of a closed-loop RL policy, we compare HUMAN2SIM2ROBOT to baselines that do not learn policies via RL. Without RL, these baselines require robot action labels for the entire task, which is achieved by performing human hand pose estimation and human-to-robot retargeting for *every* frame of the video demonstration. See Appendix H for details on baselines. We evaluate HUMAN2SIM2ROBOT against 3 baselines across 7 real-world tasks:

- **Replay:** Performs open-loop replay of the robot joint configuration trajectory by setting the joint PD targets to the retargeted joint positions.
- **Object-Aware (OA) Replay:** Like **Replay**, but warps the trajectory by the relative transform between initial object pose in the human demo and at test time (similar to PEP [51] and OKAMI [27]).
- **Behavior Cloning (BC):** Trains a closed-loop diffusion policy [8] on 30 demos (same number as HuDOR’s [16] baseline), generated from our one demo by sampling object poses (same range as our RL training), performing OA Replay, and using these trajectories as demo data.

For each real-world task, we evaluate the success of the task-specific RL policy and the corresponding baselines on 10 policy rollouts. The results are visualized in Figure 8. Across all tasks, HUMAN2SIM2ROBOT policies outperforms the baselines substantially. As we hypothesized, **Replay**’s open-loop trajectory is not successful on most tasks. **OA Replay** accounts for randomizations in initial position, but still had many failures to due to (1) hand pose estimation

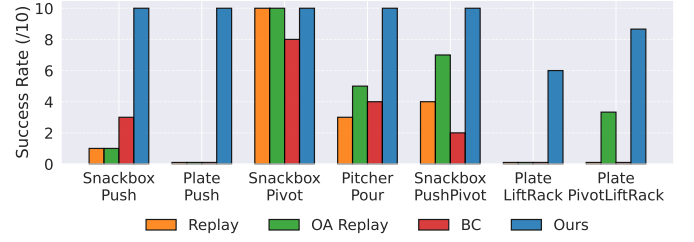


Fig. 8. **Real-World Success Rates.** HUMAN2SIM2ROBOT’s RL policies outperform Replay by 67%, Object-Aware (OA) Replay by 55%, and Behavior Cloning (BC) by 68%, across grasping, non-prehensile manipulation, and complex tasks composing multiple skill types.



Fig. 9. **Plate Pivot Lift Rack.** Robot converges on a strategy that is guided by the human demonstration, but adapted to its morphological differences.

errors that make retargeting challenging, (2) morphological differences between the human and Allegro hand, and (3) non-reactive open-loop control. It does perform well on tasks that do not require high precision like `snackbox-pivot`. **BC** performed similarly to **Replay**, which can be attributed to challenges learning from a small, lower quality dataset, as actions are computed from noisy human hand pose estimations. Despite being a closed-loop policy, small deviations from the data distribution resulted in compounding errors throughout policy rollouts. While retargeted robot demos can succeed on simpler tasks, they often fail on harder multi-step plate tasks. In contrast, HUMAN2SIM2ROBOT policies do not simply imitate the human behavior, but adapt the behavior for the robot embodiment to perform the task, resulting in much higher success rates across tasks studied in our experiments.

Regarding HUMAN2SIM2ROBOT failure modes, failures typically arose from converging on policies that exploited simulation inaccuracies or from significant pose estimation error from occlusion. Examples of simulation inaccuracies include imperfect friction modeling of the tabletop and static objects, such that policies converged on behavior that leveraged these inaccurate parameters. The most challenging task was `plate-pivot-lift-rack` (Figure 9) as it required high precision object handling: the thin plate is hard to manipulate and easily slips out of the large Allegro hand.

C. Importance of Object Pose Trajectory

We perform experiments in simulation to study the impact of the object pose trajectory-tracking reward. In particular, we study the speed and stability of learning, the final achieved reward, and the qualitative behavior. We ablate this component of our framework by comparing with the following:

- **Fixed Target:** In r_t^{obj} (Equation 1), we replace current goal object pose $T_{\tau+t}^{\text{goal}}$ with final object pose T_T^{goal} .
- **Interpolated Target:** In r_t^{obj} (Equation 1), we replace

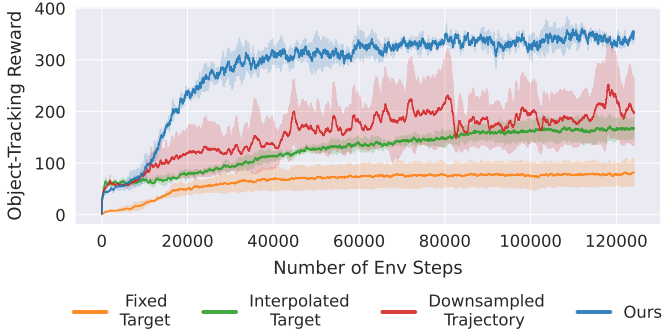


Fig. 10. **Object Pose Tracking Reward Ablation.** Reward curves comparing our approach with three approaches ablating the object pose tracking reward.

the per-timestep object goal trajectory from the demonstration $\mathbf{T}_{\tau+t}^{\text{goal}}$ with an interpolated pose trajectory between the initial and final object pose in the demonstration: $\text{POSE_INTERP}(\mathbf{T}_{\tau}^{\text{goal}}, \mathbf{T}_T^{\text{goal}}, t/(T - \tau))$, where $\text{POSE_INTERP} : \text{SE}(3) \times \text{SE}(3) \times [0, 1] \rightarrow \text{SE}(3)$ directly interpolates the position and using spherical linear interpolation for interpolating the orientation.

- **Downsampled Trajectory:** In r_t^{obj} (Equation 1), we replace the current goal object pose $\mathbf{T}_{\tau+t}^{\text{goal}}$ with the downsampled pose $\mathbf{T}_{\tau+t_{\text{down}}}^{\text{goal}}$, where $t_{\text{down}} = \lfloor t/D \rfloor \cdot D$ and D is the downsampling factor. This reduces the temporal resolution of the trajectory into a series of waypoints.

In Figure 10, we report the reward curves of the different approaches on the `plate-pivot-lift-rack` task. We train policies with three random seeds for all approaches. We see that HUMAN2SIM2ROBOT achieves a substantially higher average reward than the methods ablating the object pose tracking reward. The plate lying flat on the table is too large to be directly grasped, therefore the optimal strategy is to use extrinsic manipulation leveraging the wall to pivot the plate into a graspable position, as demonstrated in the human video. **Fixed Target** and **Interpolated Target** encourage the policy to greedily move the plate directly to the target in the air, but they struggle to pick up the plate and get stuck in a local minimum. The policy does not explore extrinsic manipulation because this requires navigating to low reward regions for a long period. **Downsampled Trajectory** is able to learn the task, but it takes longer to learn due to the weaker learning signal. It produces jerky motions in hopes of maximizing reward by tracking the waypoints that jump suddenly. **Ours** uses the full dense object pose trajectory, which ultimately achieves the strongest performance and converges the fastest, underscoring the effectiveness of an object-centric, embodiment-agnostic reward function for learning dexterous manipulation policies with RL that can be successfully deployed in the real-world.

D. Importance of Pre-Manipulation Pose Initialization

We perform experiments in simulation to study the impact of pre-manipulation hand pose initialization. In particular, we study the speed and stability of learning, the final achieved reward, and the qualitative behavior. We ablate this component of our framework by comparing with the following:

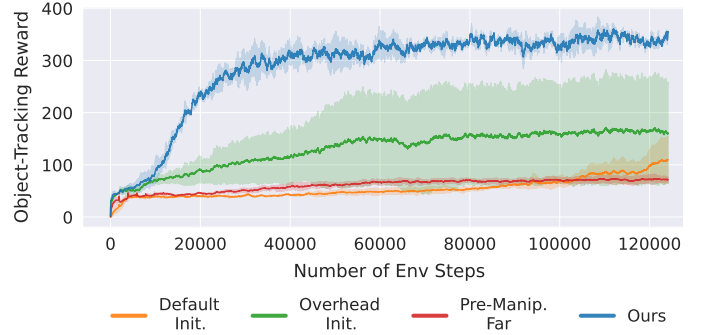


Fig. 11. **Pre-Manipulation Hand Pose Ablation.** Reward curves comparing our approach with three approaches ablating the pre-manipulation hand pose.

- **Default Initialization:** We initialize the robot configuration at a default rest pose that is not close to the object.
- **Overhead Initialization:** We compute a joint configuration with IK setting the robot palm 5cm above the object. We set the hand joint angles to a default open hand pose.
- **Pre-Manipulation Far:** We initialize the robot with the pre-manipulation hand pose, but adjust the arm joint angles to move the robot palm further 20cm away.

In Figure 11, we report the reward curves of the different approaches on the `plate-pivot-lift-rack` task. We train policies with three random seeds for all approaches. For the `plate-pivot-lift-rack` task, we see that HUMAN2SIM2ROBOT achieves a substantially higher average reward than the methods ablating the pre-manipulation pose initialization. **Default Initialization** and **Pre-Manipulation Far** perform the worst due to exploration challenges from starting with the hand too far away from the object. **Overhead Initialization** performs slightly better because it is initialized closer to the object, but fails to converge on a successful policy because the overhead grasp provides a disadvantageous prior, as it is not the optimal approach for performing the task. **Ours** ultimately results in the highest rewards by minimizing the exploration challenges and providing an advantageous initialization for faster learning.

To eliminate the need to always initialize the robot hand in close proximity to the object, methods such as collision-free motion planning or straightforward reward formulations like the L2 distance to the pre-manipulation pose have been extensively studied. These techniques can be seamlessly integrated into our system to facilitate navigation from a default rest pose to the pre-manipulation pose. The ablation tests presented here highlight the significant effectiveness of the pre-manipulation pose in guiding the RL policy toward learning human-like behaviors for contact-rich manipulation tasks.

Qualitatively, for tasks like `plate-pivot-lift-rack` that are more intricate, small differences in the pre-manipulation hand pose can result in very different learned strategies due to the differences in the human and robot morphologies. For instance, while the human hand used the pinky and ring fingers to lift the plate before transitioning to a grasp, the Allegro hand, which is much larger, used its ring finger to pivot the plate and clipped it between the middle and index finger once the plate was off the table

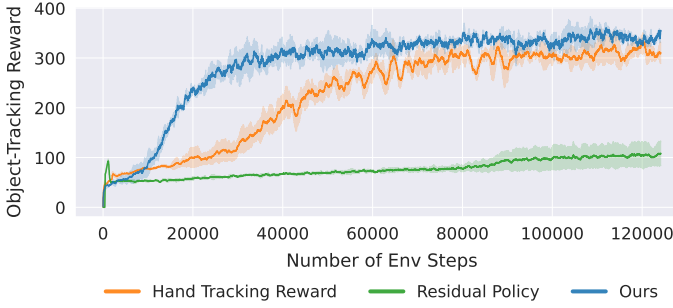


Fig. 12. **Full Hand Trajectory-Tracking Ablation.** Reward curves comparing our approach with two approaches that leverage the full hand trajectory.

(see Figure 9). This further underscores our hypothesis that significant differences in robot morphologies may lead to strategies that are guided by the human motion but ultimately converge on a different strategy that is more suitable for the robot’s embodiment after learning through trial-and-error.

E. Sufficiency of Single Pre-Manipulation Hand Pose

We perform experiments in simulation to compare pre-manipulation hand pose initialization to the following methods that require the full human hand trajectory:

- **Hand Tracking Reward:** We add a hand trajectory tracking reward term $r_t^{\text{hand}} = \exp(-\alpha \| \mathbf{X}_{\text{fingertips}} - \mathbf{X}^{\text{desired-fingertips}} \|)$ to our reward function to follow the human hand trajectory for the entire episode. Our new reward function is $r_t = r_t^{\text{obj}} + r_t^{\text{hand}}$.
- **Residual Policy:** We keep the same object-centric reward function, but now the retargeted robot configuration trajectory is replayed open-loop, and the action space learns delta PD joint target actions, inspired by Chen et al. [6].

In Figure 12, we report the reward curves of the different approaches on the `plate-pivot-lift-rack` task. We train policies with three random seeds for all approaches. We find that **Hand Tracking Reward** is able to learn an effective policy, but it learns more slowly because it initially focuses on improving its hand-tracking reward, which is not always conducive to policy performance. When trained to convergence, **Hand Tracking Reward** does not show any substantial improvement over our method, despite requiring additional data and supervision. **Residual Policy**’s performance is substantially worse because inaccurate hand pose estimation results in a poor base motion that is difficult to learn an effective residual policy for. In contrast, our method is able to effectively learn the task without the full human hand trajectory as additional supervision.

V. LIMITATIONS & FUTURE WORK

In this paper, we evaluate HUMAN2SIM2ROBOT’s ability to bridge the embodiment gap between human hands and a Kuka arm and Allegro hand. Future work could extend our evaluation to other robot hands or even substantially different arms and grippers (e.g., parallel-jaw grippers). We note that no aspects of HUMAN2SIM2ROBOT are specific to

the embodiment used in our experiments, and thus we expect it will be applicable to other robot embodiments.

In addition, HUMAN2SIM2ROBOT focuses on tasks specified by the pose trajectory of a single object. Adapting the method to handle multiple objects is possible with our framework, but would require additional modifications. HUMAN2SIM2ROBOT also assumes a high-quality object tracker (in our case, an object pose estimator) and simulator. Our tasks therefore only feature rigid-body objects and environments, which can be efficiently tracked with existing pose estimators and simulated using existing rigid-body simulators. Extending to articulated or deformable objects would necessitate adapting HUMAN2SIM2ROBOT to using different approaches for state estimation and simulation modeling.

While using 6D object pose as policy input enhances robustness against visual distractors and simplifies RL training and sim-to-real transfer, our pose estimator has limitations as it struggles with pose ambiguity of symmetric objects and sensor noise from reflective objects. Invariance to pose ambiguity of symmetric objects could be achieved by modifying the anchor points used to determine object-centric rewards, for instance by automatically determining the axis of symmetry given the object mesh [39] and removing the points orthogonal to this axis of rotation, as detailed in our reward computation definition in Section III-B. For reflective objects, these challenges can be addressed by distilling the pose-based policies into image-based policies, similar to prior work [30, 49].

Finally, HUMAN2SIM2ROBOT currently trains robust single-object, single-task policies. In future work, we can explore training generalist multi-task, multi-object policies that are conditioned on object shape and desired object trajectory. This can be achieved using multi-task RL or teacher-student distillation. Future work can also investigate extensions or modifications to HUMAN2SIM2ROBOT for bimanual manipulation or whole-body manipulation tasks.

VI. CONCLUSION

We present HUMAN2SIM2ROBOT, a real-to-sim-to-real RL framework for learning robust dexterous manipulation robot policies from a single human hand RGB-D video demonstration. Our method facilitates training RL policies in simulation for dexterous manipulation by leveraging object pose trajectories for task specification and a pre-manipulation hand pose initialization for efficient policy exploration, eliminating the need for wearables, teleoperation, or extensive data collection efforts typically required in IL. By formalizing tasks through object-centric rewards and a pre-manipulation hand pose, HUMAN2SIM2ROBOT addresses several key challenges in general dexterous manipulation, including efficient exploration, eliminating reward engineering effort, crossing the human-robot embodiment gap, and robust sim-to-real transfer. Our experiments demonstrate significant improvements over existing methods across grasping, non-prehensile manipulation, and extrinsic manipulation tasks. Overall, HUMAN2SIM2ROBOT represents a step forward in facilitating scalable, efficient, and robust training of real-world dexterous manipulation policies using sim-to-real RL with minimal human input.

ACKNOWLEDGMENTS

We thank the reviewers for their helpful suggestions and feedback. This work is supported by Stanford Human-Centered Artificial Intelligence, the National Science Foundation under Grant Numbers 2153854 and 2342246, and the Natural Sciences and Engineering Research Council of Canada (NSERC) under Award Number 526541680.

REFERENCES

- [1] Anthony Brohan, Noah Brown, Justice Carbajal, Yevgen Chebotar, Xi Chen, Krzysztof Choromanski, Tianli Ding, Danny Driess, Avinava Dubey, Chelsea Finn, Pete Florence, Chuyuan Fu, Montse Gonzalez Arenas, Keerthana Gopalakrishnan, Kehang Han, Karol Hausman, Alex Herzog, Jasmine Hsu, Brian Ichter, Alex Irpan, Nikhil Joshi, Ryan Julian, Dmitry Kalashnikov, Yuheng Kuang, Isabel Leal, Lisa Lee, Tsang-Wei Edward Lee, Sergey Levine, Yao Lu, Henryk Michalewski, Igor Mordatch, Karl Pertsch, Kanishka Rao, Krista Reymann, Michael Ryoo, Grecia Salazar, Pannag Sanketi, Pierre Sermanet, Jaspiar Singh, Anikait Singh, Radu Soricut, Huong Tran, Vincent Vanhoucke, Quan Vuong, Ayzaan Wahid, Stefan Welker, Paul Wohlhart, Jialin Wu, Fei Xia, Ted Xiao, Peng Xu, Sichun Xu, Tianhe Yu, and Brianna Zitkovich. Rt-2: Vision-language-action models transfer web knowledge to robotic control. In *arXiv preprint arXiv:2307.15818*, 2023.
- [2] Anthony Brohan, Noah Brown, Justice Carbajal, Yevgen Chebotar, Joseph Dabis, Chelsea Finn, Keerthana Gopalakrishnan, Karol Hausman, Alex Herzog, Jasmine Hsu, Julian Ibarz, Brian Ichter, Alex Irpan, Tomas Jackson, Sally Jesmonth, Nikhil Joshi, Ryan Julian, Dmitry Kalashnikov, Yuheng Kuang, Isabel Leal, Kuang-Huei Lee, Sergey Levine, Yao Lu, Utsav Malla, Deeksha Manjunath, Igor Mordatch, Ofir Nachum, Carolina Parada, Jodilyn Peralta, Emily Perez, Karl Pertsch, Jor-nell Quiambao, Kanishka Rao, Michael Ryoo, Grecia Salazar, Pannag Sanketi, Kevin Sayed, Jaspiar Singh, Sumedh Sontakke, Austin Stone, Clayton Tan, Huong Tran, Vincent Vanhoucke, Steve Vega, Quan Vuong, Fei Xia, Ted Xiao, Peng Xu, Sichun Xu, Tianhe Yu, and Brianna Zitkovich. Rt-1: Robotics transformer for real-world control at scale. In *Robotics: Science and Systems*, 2023.
- [3] Claire Chen, Zhongchun Yu, Hojung Choi, Mark Cutkosky, and Jeannette Bohg. Dexforce: Extracting force-informed actions from kinesthetic demonstrations for dexterous manipulation, 2025. URL <https://arxiv.org/abs/2501.10356>.
- [4] Sirui Chen, Chen Wang, Kaden Nguyen, Li Fei-Fei, and C Karen Liu. Arcap: Collecting high-quality human demonstrations for robot learning with augmented reality feedback. *arXiv preprint arXiv:2410.08464*, 2024.
- [5] Yuanpei Chen, Yaodong Yang, Tianhao Wu, Shengjie Wang, Xidong Feng, Jiechuan Jiang, Zongqing Lu, Stephen Marcus McAleer, Hao Dong, and Song-Chun Zhu. Towards human-level bimanual dexterous manipulation with reinforcement learning. In *Thirty-sixth Conference on Neural Information Processing Systems Datasets and Benchmarks Track*, 2022. URL <https://openreview.net/forum?id=D29JbExncTP>.
- [6] Yuanpei Chen, Chen Wang, Yaodong Yang, and Karen Liu. Object-centric dexterous manipulation from human motion data. In *8th Annual Conference on Robot Learning*, 2024.
- [7] Xuxin Cheng, Kexin Shi, Ananye Agarwal, and Deepak Pathak. Extreme parkour with legged robots. In *2024 IEEE International Conference on Robotics and Automation (ICRA)*, 2024.
- [8] Cheng Chi, Siyuan Feng, Yilun Du, Zhenjia Xu, Eric Cousineau, Benjamin Burchfiel, and Shuran Song. Diffusion policy: Visuomotor policy learning via action diffusion. In *Proceedings of Robotics: Science and Systems (RSS)*, 2023.
- [9] Cheng Chi, Zhenjia Xu, Siyuan Feng, Eric Cousineau, Yilun Du, Benjamin Burchfiel, Russ Tedrake, and Shuran Song. Diffusion policy: Visuomotor policy learning via action diffusion. In *Robotics: Science and Systems*, 2023.
- [10] Cheng Chi, Zhenjia Xu, Chuer Pan, Eric Cousineau, Benjamin Burchfiel, Siyuan Feng, Russ Tedrake, and Shuran Song. Universal manipulation interface: In-the-wild robot teaching without in-the-wild robots. In *Proceedings of Robotics: Science and Systems (RSS)*, 2024.
- [11] Matei T. Ciocarlie, Corey Goldfeder, and Peter K. Allen. Dexterous grasping via eigengrasps : A low-dimensional approach to a high-complexity problem. 2007. URL <https://api.semanticscholar.org/CorpusID:6853822>.
- [12] Open X-Embodiment Collaboration. Open X-Embodiment: Robotic learning datasets and RT-X models. In *2024 IEEE International Conference on Robotics and Automation (ICRA)*, pages 6892–6903, 2024. doi: 10.1109/ICRA57147.2024.10611477.
- [13] Erwin Coumans and Yunfei Bai. Pybullet, a python module for physics simulation for games, robotics and machine learning. <http://pybullet.org>, 2016–2019.
- [14] Sudeep Dasari, Abhinav Gupta, and Vikash Kumar. Learning dexterous manipulation from exemplar object trajectories and pre-grasps. In *2023 IEEE International Conference on Robotics and Automation (ICRA)*, pages 3889–3896. IEEE, 2023.
- [15] Michael Drolet, Simon Stepputtis, Siva Kailas, Ajinkya Jain, Jan Peters, Stefan Schaal, and Heni Ben Amor. A comparison of imitation learning algorithms for bimanual manipulation. *IEEE Robotics and Automation Letters (RA-L)*, 2024.
- [16] Irmak Guzey, Yinlong Dai, Georgy Savva, Raunaq Bhirangi, and Lerrel Pinto. Bridging the human to robot dexterity gap through object-oriented rewards. In *arXiv preprint arXiv:2410.23289*, 2024. URL <https://arxiv.org/abs/2410.23289>.
- [17] Tuomas Haarnoja, Ben Moran, Guy Lever, Sandy H. Huang, Dhruva Tirumala, Jan Humplik, Markus Wulfmeier, Saran Tunyasuvunakool, Noah Y.

- Siegel, Roland Hafner, Michael Bloesch, Kristian Hartikainen, Arunkumar Byravan, Leonard Hasenclever, Yuval Tassa, Fereshteh Sadeghi, Nathan Batchelor, Federico Casarini, Stefano Saliceti, Charles Game, Neil Sreendra, Kushal Patel, Marlon Gwira, Andrea Huber, Nicole Hurley, Francesco Nori, Raia Hadsell, and Nicolas Heess. Learning agile soccer skills for a bipedal robot with deep reinforcement learning. *Science Robotics*, 9(89):eadi8022, 2024. doi: 10.1126/scirobotics.adi8022. URL <https://www.science.org/doi/abs/10.1126/scirobotics.adi8022>.
- [18] Nick Heppert, Max Argus, Tim Welschhold, Thomas Brox, and Abhinav Valada. Ditto: Demonstration imitation by trajectory transformation. In *2024 IEEE/RSJ International Conference on Intelligent Robots and Systems (IROS)*. IEEE, 2024.
- [19] Eric Jang, Alex Irpan, Mohi Khansari, Daniel Kappler, Frederik Ebert, Corey Lynch, Sergey Levine, and Chelsea Finn. BC-z: Zero-shot task generalization with robotic imitation learning. In *5th Annual Conference on Robot Learning*, 2021. URL <https://openreview.net/forum?id=8kbp23tSGYv>.
- [20] Zhenyu Jiang, Yuqi Xie, Kevin Lin, Zhenjia Xu, Weikang Wan, Ajay Mandalekar, Linxi Fan, and Yuke Zhu. Dexmimicgen: Automated data generation for bimanual dexterous manipulation via imitation learning. In *arXiv preprint arXiv:2410.24185*, 2024.
- [21] Elia Kaufmann, Leonard Bauersfeld, Antonio Loquercio, Matthias Mueller, Vladlen Koltun, and Davide Scaramuzza. Champion-level drone racing using deep reinforcement learning. In *Nature*, volume 620, pages 982–987, 2023.
- [22] Justin Kerr, Chung Min Kim, Mingxuan Wu, Brent Yi, Qianqian Wang, Ken Goldberg, and Angjoo Kanazawa. Robot see robot do: Imitating articulated object manipulation with monocular 4d reconstruction. In *8th Annual Conference on Robot Learning*, 2024. URL <https://openreview.net/forum?id=2LLu3gavF1>.
- [23] Moo Jin Kim, Karl Pertsch, Siddharth Karamcheti, Ted Xiao, Ashwin Balakrishna, Suraj Nair, Rafael Rafailov, Ethan Foster, Grace Lam, Pannag Sanketi, Quan Vuong, Thomas Kollar, Benjamin Burchfiel, Russ Tedrake, Dorsa Sadigh, Sergey Levine, Percy Liang, and Chelsea Finn. Openvla: An open-source vision-language-action model. *8th Annual Conference on Robot Learning*, 2024.
- [24] KIRI Innovation (Hongkong) Limited. Kiri Engine: 3D Scanner App, 2024. URL <https://www.kiriengine.app>. Available for Android, iOS, and Web.
- [25] Sateesh Kumar, Jonathan Zamora, Nicklas Hansen, Rishabh Jangir, and Xiaolong Wang. Graph inverse reinforcement learning from diverse videos. *Conference on Robot Learning (CoRL)*, 2022.
- [26] Laan Labs. 3D Scanner App: LiDAR Scanner for iPad and iPhone Pro, 2024. URL <https://3dscannerapp.com>. Available for iOS devices.
- [27] Jinhan Li, Yifeng Zhu, Yuqi Xie, Zhenyu Jiang, Mingyao Seo, Georgios Pavlakos, and Yuke Zhu. Okami: Teaching humanoid robots manipulation skills through single video imitation. In *8th Annual Conference on Robot Learning (CoRL)*, 2024.
- [28] Fanqi Lin, Yingdong Hu, Pingyue Sheng, Chuan Wen, Jiacheng You, and Yang Gao. Data scaling laws in imitation learning for robotic manipulation, 2024. URL <https://arxiv.org/abs/2410.18647>.
- [29] Shilong Liu, Zhaoyang Zeng, Tianhe Ren, Feng Li, Hao Zhang, Jie Yang, Chunyuan Li, Jianwei Yang, Hang Su, Jun Zhu, et al. Grounding dino: Marrying dino with grounded pre-training for open-set object detection. *arXiv preprint arXiv:2303.05499*, 2023.
- [30] Tyler Ga Wei Lum, Martin Matak, Viktor Makoviychuk, Ankur Handa, Arthur Allshire, Tucker Hermans, Nathan D. Ratliff, and Karl Van Wyk. DextrAH-g: Pixels-to-action dexterous arm-hand grasping with geometric fabrics. In *8th Annual Conference on Robot Learning*, 2024. URL <https://openreview.net/forum?id=S2Jwb0i7HN>.
- [31] Zhengyi Luo, Jinkun Cao, Sammy Christen, Alexander Winkler, Kris Kitani, and Weipeng Xu. Grasping diverse objects with simulated humanoids, 2024. URL <https://arxiv.org/abs/2407.11385>.
- [32] Raymond R. Ma and Aaron M. Dollar. On dexterity and dexterous manipulation. In *2011 15th International Conference on Advanced Robotics (ICAR)*, pages 1–7, 2011. doi: 10.1109/ICAR.2011.6088576.
- [33] Denys Makoviichuk and Viktor Makoviychuk. rl-games: A high-performance framework for reinforcement learning. https://github.com/Denys88/rl_games, May 2021.
- [34] Viktor Makoviychuk, Lukasz Wawrzyniak, Yunrong Guo, Michelle Lu, Kier Storey, Miles Macklin, David Hoeller, Nikita Rudin, Arthur Allshire, Ankur Handa, and Gavriel State. Isaac gym: High performance gpu-based physics simulation for robot learning, 2021. URL <https://arxiv.org/abs/2108.10470>.
- [35] Gabriel Margolis, Ge Yang, Kartik Paigwar, Tao Chen, and Pulkit Agrawal. Rapid locomotion via reinforcement learning. In *Robotics: Science and Systems*, 2022.
- [36] Takahiro Miki, Joonho Lee, Jemin Hwangbo, Lorenz Wellhausen, Vladlen Koltun, and Marco Hutter. Learning robust perceptive locomotion for quadrupedal robots in the wild. *Science Robotics*, 7(62):eabk2822, 2022. doi: 10.1126/scirobotics.abk2822. URL <https://www.science.org/doi/abs/10.1126/scirobotics.abk2822>.
- [37] William Noll, Yen-Hsun Wu, and Marco Santello. Dexterous manipulation: Differential sensitivity of manipulation and grasp forces to task requirements. *Journal of neurophysiology*, 132, 06 2024. doi: 10.1152/jn.00034.2024.
- [38] Georgios Pavlakos, Dandan Shan, Ilija Radosavovic, Angjoo Kanazawa, David Fouhey, and Jitendra Malik. Reconstructing hands in 3D with transformers. In *CVPR*, 2024.
- [39] Soo-Chang Pei and Lin-Gwo Liou. Automatic symmetry determination and normalization for rotationally symmetric 2d shapes and 3d solid objects. *Pattern Recognition*, 27(9):1193–1208, 1994. ISSN 0031-3203. doi: [https://doi.org/10.1016/0031-3203\(94](https://doi.org/10.1016/0031-3203(94)

- 90005-1. URL <https://www.sciencedirect.com/science/article/pii/S0031320394900051>.
- [40] Lerrel Pinto, Marcin Andrychowicz, Peter Welinder, Wojciech Zaremba, and Pieter Abbeel. Asymmetric actor critic for image-based robot learning. In Hadas Kress-Gazit, Siddhartha S. Srinivasa, Tom Howard, and Nikolay Atanasov, editors, *Robotics: Science and Systems XIV, Carnegie Mellon University, Pittsburgh, Pennsylvania, USA, June 26-30, 2018*, 2018. doi: 10.15607/RSS.2018.XIV.008. URL <http://www.roboticsproceedings.org/rss14/p08.html>.
- [41] Haozhi Qi, Ashish Kumar, Roberto Calandra, Yi Ma, and Jitendra Malik. In-Hand Object Rotation via Rapid Motor Adaptation. In *Conference on Robot Learning (CoRL)*, 2022.
- [42] Yuzhe Qin, Yueh-Hua Wu, Shaowei Liu, Hanwen Jiang, Ruihan Yang, Yang Fu, and Xiaolong Wang. Dexmv: Imitation learning for dexterous manipulation from human videos, 2021.
- [43] Aravind Rajeswaran, Vikash Kumar, Abhishek Gupta, Giulia Vezzani, John Schulman, Emanuel Todorov, and Sergey Levine. Learning Complex Dexterous Manipulation with Deep Reinforcement Learning and Demonstrations. In *Proceedings of Robotics: Science and Systems (RSS)*, 2018.
- [44] Nikhila Ravi, Valentin Gabeur, Yuan-Ting Hu, Ronghang Hu, Chaitanya Ryali, Tengyu Ma, Haitham Khedr, Roman Rädle, Chloe Rolland, Laura Gustafson, Eric Mintun, Junting Pan, Kalyan Vasudev Alwala, Nicolas Carion, Chao-Yuan Wu, Ross Girshick, Piotr Dollár, and Christoph Feichtenhofer. Sam 2: Segment anything in images and videos. *arXiv preprint arXiv:2408.00714*, 2024. URL <https://arxiv.org/abs/2408.00714>.
- [45] Javier Romero, Dimitrios Tzionas, and Michael J. Black. Embodied hands: Modeling and capturing hands and bodies together. *ACM Transactions on Graphics, (Proc. SIGGRAPH Asia)*, 36(6), November 2017.
- [46] John Schulman, Filip Wolski, Prafulla Dhariwal, Alec Radford, and Oleg Klimov. Proximal policy optimization algorithms. *arXiv preprint arXiv:1707.06347*, 2017.
- [47] Himanshu Gaurav Singh, Antonio Loquercio, Carmelo Sferrazza, Jane Wu, Haozhi Qi, Pieter Abbeel, and Jitendra Malik. Hand-object interaction pretraining from videos, 2024. URL <https://arxiv.org/abs/2409.08273>.
- [48] Balakumar Sundaralingam, Siva Kumar Sastry Hari, Adam Fishman, Caelan Garrett, Karl Van Wyk, Valts Blukis, Alexander Millane, Helen Oleynikova, Ankur Handa, Fabio Ramos, Nathan Ratliff, and Dieter Fox. curobo: Parallelized collision-free minimum-jerk robot motion generation, 2023.
- [49] Marcel Torne, Anthony Simeonov, Zechu Li, April Chan, Tao Chen, Abhishek Gupta, and Pulkrit Agrawal. Reconciling reality through simulation: A real-to-sim-to-real approach for robust manipulation. *Arxiv*, 2024.
- [50] Eugene Valassakis, Georgios Papagiannis, Norman Di Palo, and Edward Johns. Demonstrate once, imitate immediately (dome): Learning visual servoing for one-shot imitation learning. In *IEEE/RSJ International Conference on Intelligent Robots and Systems (IROS)*, 2022.
- [51] Pietro Vitiello, Kamil Dreczkowski, and Edward Johns. One-shot imitation learning: A pose estimation perspective. In *Conference on Robot Learning*, 2023.
- [52] Weikang Wan, Haoran Geng, Yun Liu, Zikang Shan, Yaodong Yang, Li Yi, and He Wang. Unidexgrasp++: Improving dexterous grasping policy learning via geometry-aware curriculum and iterative generalist-specialist learning. *arXiv preprint arXiv:2304.00464*, 2023.
- [53] Chen Wang, Haochen Shi, Weizhuo Wang, Ruohan Zhang, Li Fei-Fei, and C. Karen Liu. Dexcap: Scalable and portable mocap data collection system for dexterous manipulation. *Robotics: Science and Systems*, 2024.
- [54] Bowen Wen, Wei Yang, Jan Kautz, and Stan Birchfield. Foundationpose: Unified 6d pose estimation and tracking of novel objects. In *Proceedings of the IEEE/CVF Conference on Computer Vision and Pattern Recognition (CVPR)*, pages 17868–17879, June 2024.
- [55] Yinzhen Xu, Weikang Wan, Jialiang Zhang, Haoran Liu, Zikang Shan, Hao Shen, Ruicheng Wang, Haoran Geng, Yijia Weng, Jiayi Chen, et al. Unidexgrasp: Universal robotic dexterous grasping via learning diverse proposal generation and goal-conditioned policy. *arXiv preprint arXiv:2303.00938*, 2023.
- [56] Jianglong Ye, Jiashun Wang, Binghao Huang, Yuzhe Qin, and Xiaolong Wang. Learning continuous grasping function with a dexterous hand from human demonstrations. *IEEE Robotics and Automation Letters*, 2023.
- [57] Seonghyeon Ye, Joel Jang, Byeongguk Jeon, SeJune Joo, Jianwei Yang, Baolin Peng, Ajay Mandlekar, Reuben Tan, Yu-Wei Chao, Bill Yuchen Lin, Lars Liden, Kimin Lee, Jianfeng Gao, Luke Zettlemoyer, Dieter Fox, and Minjoon Seo. Latent action pretraining from videos, 2024. URL <https://arxiv.org/abs/2410.11758>.
- [58] Kevin Zakka, Andy Zeng, Pete Florence, Jonathan Tompson, Jeannette Bohg, and Debidatta Dwibedi. Xirl: Cross-embodiment inverse reinforcement learning. *Conference on Robot Learning (CoRL)*, 2021.
- [59] Tony Z. Zhao, Jonathan Tompson, Danny Driess, Pete Florence, Seyed Kamyar Seyed Ghasemipour, Chelsea Finn, and Ayzaan Wahid. ALOHA unleashed: A simple recipe for robot dexterity. In *8th Annual Conference on Robot Learning*, 2024. URL <https://openreview.net/forum?id=gvdXE7ikHI>.
- [60] Henry Zhu, Justin Yu, Abhishek Gupta, Dhruv Shah, Kristian Hartikainen, Avi Singh, Vikash Kumar, and Sergey Levine. The ingredients of real-world robotic reinforcement learning, 2020. URL <https://arxiv.org/abs/2004.12570>.

APPENDIX

A. Real-to-Sim & Human Demo Processing Details

1) *Digital Twin Construction Details:* In this section, we describe the construction of the digital twin simulation environment (i.e., real-to-sim) and how we process the human demonstration. We start by taking a scan of the real-world environment for transfer to simulation. We used the off-the-shelf LiDAR scanning app called 3D Scanner App [26] to perform a detailed scene scan of the workspace (including static objects on the tabletop) and the robot. We then used this scene scan to align the robot, tabletop, and static objects in our digital twin simulation. The scene scan took ~ 3 minutes and alignment of the assets in simulation took another ~ 2 minutes. This process was performed once and the same simulation environment was used for all tasks. Next, we need to take an object scan to obtain the object mesh used for object pose tracking. We use another off-the-shelf LiDAR scanning app called Kiri Engine [24] to do this, as we find it is better for scanning small objects than the 3D Scanner App (conversely, 3D Scanner App seems to perform better for larger scene scans than Kiri Engine). This takes ~ 2 minutes per object, and we only need to do this once per object used in our experiments. All relevant code for real-to-sim pipeline can be found here.

2) *Human Demo Processing Details:* For processing the human demonstration, each task takes 0.5 minutes to obtain an RGB-D video demonstration. The human demonstration is then processed in three steps: (i) generating the per-frame object and hand masks using SAM 2 [44]; (ii) generating the object pose trajectory by passing in the RGB-D video frames, object segmentation mask frames, and object mesh into FoundationPose [54]; (iii) obtaining the pre-manipulation hand pose by passing the corresponding RGB frame into HaMeR [38], then performing depth alignment with the segmented hand depth values, which we describe in the following section.

3) *Depth Alignment of HaMeR Hand Pose Estimates:* HaMeR [38] predicts MANO hand pose and shape parameters from a single RGB image. While its 2D projections are generally reliable, the absence of depth information leads to significant 3D errors, which can be as large as 20–30 cm, particularly when the hand is far from the camera. Such discrepancies result in suboptimal pre-manipulation hand poses, adversely affecting reinforcement learning (RL) initialization and methods that require a full human hand trajectory.

To address this issue, we incorporate depth information to refine HaMeR’s hand pose predictions. First, we obtain the initial MANO hand estimate from HaMeR. Next, we generate a hand segmentation mask using SAM 2 [44] and extract the corresponding 3D hand points from the depth image using the camera parameters. Next, we compute the 3D positions of the predicted MANO hand vertices visible to the camera and use a clustering algorithm to filter out erroneous depth points. Specifically, we construct a KD-tree from the extracted 3D points and identify pairs of points within 5 cm using nearest-neighbor queries. We then represent these points as a graph, where edges connect nearby points. We assume that the hand point cloud is the largest connected component, so we only retain the points in this connected graph, which mitigates the

impact of depth noise and segmentation errors from the arm or background. Finally, we apply Iterative Closest Point (ICP) registration to align the MANO prediction with the segmented depth-based point cloud. This approach effectively improves alignment in most frames. However, accuracy degrades when significant occlusions occur, such as when fingers grasp around an object and face away from the depth camera.

In total, demonstration processing takes ~ 5 -10 minutes, with only a few seconds of human effort. All relevant code for processing human video demonstrations can be found here.

B. Human-to-Robot Retargeting Details

To perform arm IK, we use the parallelized IK solver provided by cuRobo [48]. The solver generates 100 unique solutions, each seeded with 20 joint configurations. These configurations consist of a selected joint configuration combined with random noise sampled from a normal distribution with a standard deviation of 15 degrees. From these solutions, we select the one closest to the selected joint configuration that meets the desired target within 5 cm for position and 3 degrees for orientation. The pose target is the position of middle knuckle (called “middle_0”) with a 3cm offset in the negative direction of the palm normal and a 3cm offset in the negative direction of the wrist to middle knuckle, and the orientation of the wrist (called “global_orient”) with a rotation offset accounting for the difference in orientation convention of the wrist and middle knuckle.

For hand IK, we use PyBullet’s IK solver [13]. The Allegro hand is moved to the pose achieved by the previous arm IK solution, after which we solve IK for each finger to reach the specified fingertip targets. A default hand pose is used as the rest pose. Since achieving precise alignment with all fingertip targets is not always possible, PyBullet’s solver provides reasonable solutions in these cases, whereas cuRobo’s solver may yield poor results when it fails. We use position targets at the human hand fingertips (called “index_3”, “middle_3”, “ring_3”, and “thumb_3”) with no adjustments.

To retarget the pre-manipulation hand pose, we execute the above process once, using the default upright arm configuration to seed the solver and selecting the best solution. During this step, we apply collision-free arm IK to ensure the robot avoids contact with the environment or objects, as this joint configuration should not be in collision.

For retargeting the full hand pose trajectory, we iteratively solve for each hand pose, using the previously computed solution as the selected joint configuration to seed the solver. This approach ensures consistency in joint angles between frames, resulting in smoother motion. While solving, we enforce collision-free arm IK to avoid contact with the environment. However, we do not enforce object collision avoidance, as contact with the object is often necessary and both hand and object pose estimates are imperfect. If the IK process fails for a particular pose, we skip that index and proceed to the next one, keeping track of the corresponding timesteps. When evaluating solutions, we select the one closest to the selected joint configuration based on the infinity norm, $\|q_{\text{solution}} - q_{\text{selected}}\|_{\infty}$.

After retargeting the full hand pose trajectory, we modify the trajectory to ensure smoothness. At each timestep, we compute

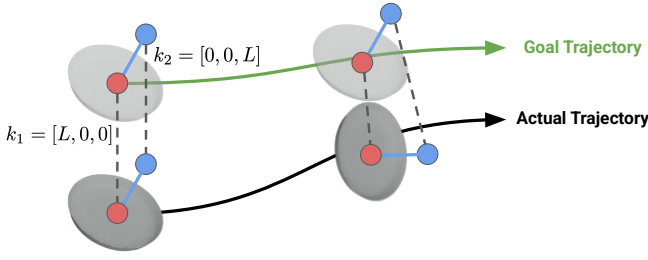


Fig. 13. **Modifying Anchor Points.** For rotationally symmetric objects, we can remove all anchor points orthogonal to the axis of symmetry (which can be determined automatically [39]). This modified object pose representation can be used for both reward computation and policy observation.

the arm joint velocity with first-order finite-differencing. If any arm joint velocity exceeds its velocity limit (indicating a discontinuity or sudden jump in joint positions within a short time period), we increase the time interval between those points and interpolate the intermediate values. This ensures that the joint velocity limits are respected, resulting in a smooth trajectory that can be safely executed on the robot.

C. Modifying Anchor Points

Figure 13 shows how anchor points can be modified to accommodate rotational invariance for rotationally symmetric objects. Our use of anchor points is a very flexible representation to parameterize a pose tracking reward function.

D. Real-Time Perception Details

In this section, we describe our real-time perception pipeline, which enables pose estimation at 30Hz using FoundationPose [54]. The process begins with pose registration to determine the object’s initial pose, which takes approximately 1 second. This step requires a textured object mesh and a segmented object mask. To generate the mask, we pass the image and a text prompt into Grounding DINO [29] to obtain an object bounding box. The image and bounding box are then passed to SAM2 [44], which produces a high-quality segmented object mask. The text prompt can either be manually provided or automatically generated by rendering the textured object mesh into an image and using GPT-4o to produce a descriptive prompt.

Once the initial pose is established, FoundationPose performs real-time object pose tracking by generating pose hypotheses near the previous estimate and selecting the best match, achieving a consistent 30Hz rate. Although this tracking is generally robust, it can fail when the object moves rapidly or becomes heavily occluded, leading to degraded pose estimates. To address this, we implement a separate pose evaluation process that monitors the quality of the pose estimates and triggers re-registration if needed.

This evaluation is performed by running SAM 2 at 1Hz to produce high-quality segmented object masks, which are treated as ground truth due to SAM 2’s reliability, even under challenging conditions. The predicted object mask, generated using FoundationPose’s pose estimate and the known camera parameters, is compared to the ground-truth mask using the

intersection over union (IoU) metric. If the IoU falls below 0.1, FoundationPose reinitializes the pose registration process.

E. Initial State Distribution Sampling

In this section, we describe sampling the initial state distribution for RL training in simulation. We sample the object pose as $T_1^{\text{obj}} = T_{\tau}^{\text{goal}} T^{\text{random}}$, where $T^{\text{random}} \in \text{SE}(3)$ is random pose noise. The rotation component of T^{random} is sampled as roll, pitch, and yaw angles from $r, p, y \sim \mathcal{U}(-\theta_{\max}, \theta_{\max})$, where $\theta_{\max} = 20^\circ$. The translation component of T^{random} is sampled as $t_x, t_y, t_z \sim \mathcal{U}(-t_{\max}, t_{\max})$, where $t_{\max} = 0.1m$ is the maximum displacement. Next, we compute the relative transformation $T^{\text{relative}} = (T^{\text{obj}})^{-1} T^{\text{wrist}}$ to determine the new pre-manipulation wrist pose as $T_1^{\text{obj}} T^{\text{relative}}$. A small amount of noise is added to the new wrist pose and hand joint angles.

F. Simulation Training Details

We train our policy using Isaac Gym [34], a high-performance GPU-accelerated simulator that enables the parallel simulation of 4096 robots per GPU. Each policy is trained on a single NVIDIA A100 GPU with 40 GB of VRAM. This configuration allows us to achieve a simulation speed of approximately 7k frames per second (FPS). Each frame corresponds to a single action step with a control timestep of 66.7 ms (15 Hz), subdivided into 8 simulation timesteps of 8.33 ms (120 Hz).

Our training duration ranges from approximately 5 to 24 hours wall-clock time depending on the task, amounting to around 0.6 billion frames, which corresponds to roughly one year of simulated experience (0.6B / 15 / 3600 / 24 / 365).

We train our policies using Proximal Policy Optimization (PPO) [46] with rl-games [33], a highly optimized GPU-based implementation that employs vectorized observations and actions for efficient training. The policy is trained with a learning rate of 5×10^{-4} , a discount factor $\gamma = 0.998$, an entropy coefficient of 0, and a PPO clipping parameter $\epsilon_{\text{clip}} = 0.2$. Additionally, we normalize observations, value estimates, and advantages, and train the policy using four mini-epochs per policy update.

We use $\alpha = 10$, $L = 0.2m$, and $t_{\text{offset}} = 30$ (at 30Hz, 1 second) by default (though we slightly vary t_{offset} depending on how quickly the human demonstration was performed).

Although our control policies will not have access to privileged simulation state information when deployed in the real world, we can still use privileged information to accelerate training in simulation. We use Asymmetric Actor Critic training [40], in which our critic $V(s)$ is given all privileged state information s and our policy $\pi(o)$ is provided an observation o , which is a limited subset of this privileged state information. With this method, the policy learns to perform the task using only the observations we can capture in the real world, but the critic can still leverage privileged state information to provide more accurate value estimates, improving the speed and quality of policy training.

The state at timestep t , s_t is defined as

$$s_t = [o_t, v_t, \omega_t, t, f_t^{\text{dof}}, F_t^{\text{fingers}}] \quad (5)$$

where \mathbf{o}_t is the observation, $\mathbf{v}_t \in \mathbb{R}^3$ is the object linear velocity, $\boldsymbol{\omega}_t \in \mathbb{R}^3$ is the object angular velocity, $t \in \mathbb{R}$ is current timestep, $\mathbf{f}_t^{\text{dof}} \in \mathbb{R}^{N^{\text{joints}}}$ is the vector of robot joint forces, and $\mathbf{F}_t^{\text{fingers}} \in \mathbb{R}^{N^{\text{fingers}}}$ contains fingertip contact forces.

Training uses horizon length of 16 (i.e., number of timesteps between updates for each robot, with all robots running in parallel) and 4096 parallel agents. The policy architecture consists of a multi-layer perceptron (MLP) with hidden layers of size [512, 512], an LSTM module with 1024 hidden units, and a critic network with hidden layers of size [1024, 512].

To improve the robustness and generalization of our policy, we apply extensive domain randomization during training. Randomizations are applied every 720 simulation steps and include variations in observations, actions, physics parameters, and object properties. Gaussian noise with a standard deviation of 0.01 is added to both observations and actions. Gravity is perturbed additively using Gaussian noise with a standard deviation of 0.3. The scale, mass, and friction of the object and table are randomized with a scaling parameter sampled from [0.7, 1.3]. The robot’s scale, damping, stiffness, friction, and mass are also randomized with a scaling parameter sampled from [0.7, 1.3]. We also introduce random force perturbations to the object. At each timestep, there is a 5% probability of applying a force with a magnitude equal to 50 times the object’s mass, directed along a randomly sampled unit vector. These perturbations serve two key purposes. First, they can displace the object before the robot makes contact, simulating real-world uncertainties such as unexpected disturbances or pose estimation errors. This encourages the policy to actively track and reach for objects that may not be precisely where they were initially observed. Second, if the object is already grasped, these perturbations can destabilize the grasp, promoting the development of robust and stable grasping strategies that minimize the likelihood of dropping the object.

All relevant code for PPO can be found [here](#), and for simulation training found [here](#).

G. Full Task List

We perform experiments on the following tasks:

- **snackbox-push**: The objective is to push the snackbox across the table until it makes contact with a static box. The snackbox is initialized in a face-down orientation, with its position randomized within a 4 cm \times 4 cm region. The task is considered successful if the snackbox reaches and contacts the static box.
- **plate-push**: Similar to **snackbox-push**, this task requires pushing a plate across the table until it contacts the static box. The plate starts in a flat orientation, with position randomized within a 4cm \times 4cm region. Success is achieved when the plate contacts the static box.
- **snackbox-pivot**: The goal is to pivot the snackbox from a face-down orientation to a sideways orientation using the static box for support. The snackbox is initialized face-down, with its position randomized within a 1cm \times 4cm region. Due to the robot’s initial position, the snackbox cannot be substantially moved in one direction. The task is successful if the snackbox is pivoted against the static box into a stable sideways orientation.

- **pitcher-pour**: This task involves grasping a pitcher by its handle, lifting it off the table, and reorienting it so that its spout is positioned above a static saucepan, simulating a pouring motion. The pitcher starts upright, with its position randomized within a 4cm \times 4cm region. The task is successful if the pitcher is lifted by its handle and positioned with its spout above the saucepan.
- **snackbox-push-pivot**: This task combines the **snackbox-push** and **snackbox-pivot** tasks. The snackbox starts in a face-down orientation, with its position randomized within a 4cm \times 4cm region. The task consists of two sequential steps. The push task is successful if the snackbox is first pushed to make contact with the static box, and the pivot task is successful if the snackbox is pivoted against the box into a sideways orientation. Success is graded on a three-level scale. The score is 0 if the push fails, 0.5 if the push succeeds but the pivot fails, and 1 if both push and pivot are successful.
- **plate-lift-rack**: The objective is to lift a plate and place it into a dishrack. The plate starts in an upright orientation, leaning against the static box, with its position randomized within a 0.5 cm \times 4 cm region. Since the plate must remain leaning against the box, its movement is primarily constrained along the box length. The task consists of two sequential steps. The lift task is successful if the plate is lifted off of the table, and the rack task is successful if the plate is placed into the dishrack while maintaining an upright orientation. Success is graded on a three-level scale. The score is 0 if the lift fails, 0.5 if the lift is successful but the rack fails, and 1 if both the lift and rack are successful.
- **plate-pivot-lift-rack**: The task consists of three sequential steps pivoting a plate against the static box, lifting it off the table, and placing it into a dishrack. The plate starts flat next to the static box, with its position randomized within a 0.5cm \times 4cm region. The pivot task is successful if the plate is pivoted against the static box to an upright orientation, the lift task is successful if the plate is lifted off of the table, and the rack task is successful if the plate is placed into the dishrack while maintaining an upright orientation. The score is 0 if the pivot fails, 0.33 if the pivot is successful but the lift fails, 0.66 if the pivot and lift are successful but the rack fails, and 1 if the pivot, lift, and rack are successful.

H. Baseline Details

1) *Full Human Hand Trajectory Estimation*: Our baseline methods typically require robot action labels for every step of the task. When working with only a single human video demonstration, this can be done by estimating the human hand pose in each frame and retargeting it to the robot. Specifically, we first perform hand pose estimation using HaMeR, followed by a depth alignment step (Appendix A). The hand poses are mapped to robot joint configurations using an inverse kinematics (IK) procedure similar to that in Section III-A.

However, simply solving the IK for each frame independently and stitching the results together often fails due to

three main issues: errors in hand pose estimation, a lack of consistency/smoothness over time, and unreachable target poses. We address these issues as follows:

- 1) **Mitigating Hand Pose Errors.** Hand pose estimation can suffer from large errors when fingers are occluded (Appendix A). To address this, we compare each newly estimated pose with the previous pose. If their distance exceeds a threshold, we skip the current frame’s pose rather than attempting to retarget an unreliable estimate.
- 2) **Ensuring Joint Consistency.** To maintain smooth transitions between consecutive poses, we iteratively solve IK using the previous solution as both a default and a seed configuration. We employ cuRobo [48] to generate 100 parallel solutions, each initialized by adding Gaussian noise (15° standard deviation) to the previous IK solution. We then select the solution whose joint angles have the smallest ℓ_∞ difference from the previous timestep’s configuration. If even this “best” solution differs excessively, we skip that frame.
- 3) **Handling Unreachable Targets.** If the IK target is unreachable, we skip the corresponding frame.

After applying these checks, we downsample the resulting trajectory and verify that all joint velocities remain below the robot’s limits. If any exceed the limit, we stretch the time between successive waypoints to reduce velocity. Although this procedure generally yields a plausible trajectory, inaccuracies can still arise in cases of severe finger occlusion or when the hand is far from the camera. In contrast, obtaining a reliable pre-manipulation hand pose is generally easier, as it requires only a single frame with accurate hand pose estimation. Such a frame is easier to find because the hand is typically not heavily occluded when it approaches the object, while the full demonstration can include much more occlusion of the hand.

2) *Replay Details:* In this section, we provide additional details on the implementation of replay. First, we need to clearly define the frames we care about. We define $T^{A \rightarrow B}$ as the relative transformation of frame B with respect to frame A . This means $T^{A \rightarrow C} = T^{A \rightarrow B} T^{B \rightarrow C}$.

Let R be the robot’s base frame, M be the robot’s middle-finger frame, C be the camera frame, and O be the object frame. Given these four frames, we need three independent relative transforms to fully specify this system. The camera extrinsics calibration gives us $T^{R \rightarrow C}$. FoundationPose object pose estimates give us $T^{C \rightarrow O}$ at each timestep. HaMeR with depth refinement gives us hand pose estimates that allow us to compute the desired pose of the robot’s middle-finger frame $T^{C \rightarrow M}$. This fully specifies the demonstration. This allows us to compute the object trajectory $\{T_t^{R \rightarrow O}\}_{t=1}^T$ and the robot’s middle-finger trajectory $\{T_t^{R \rightarrow M}\}_{t=1}^T$ for this demonstration. This is used to perform the inverse kinematics procedure described above to generate a robot configuration trajectory.

To execute replay in the real world, we can directly track this joint trajectory with joint PD control.

3) *Object-Aware Replay Details:* For object-aware replay, at timestep $t = 1$, we use FoundationPose to estimate the new object pose $T_1^{R \rightarrow O^{\text{new}}}$, which will be similar but not identical to the initial object pose during demonstration collection $T_1^{R \rightarrow O}$. Our goal is to compute a new robot middle-finger trajectory

$\{T_t^{R \rightarrow M^{\text{new}}}\}_{t=1}^T$ that keeps the same relative pose between the object and the middle-finger as in the demonstration.

Let $T^{O \rightarrow M}$ be the relative pose between the object and the middle-finger at each timestep of the demonstration. This can be computed as $T^{O \rightarrow M} = (T^{R \rightarrow O})^{-1} T^{R \rightarrow M}$. Our goal is to maintain this same relative relationship during replay, such that $T^{O \rightarrow M} = T^{O^{\text{new}} \rightarrow M^{\text{new}}}$.

The new middle-finger trajectory can then be computed as:

$$T_t^{R \rightarrow M^{\text{new}}} = T_t^{R \rightarrow O^{\text{new}}} T_t^{O^{\text{new}} \rightarrow M^{\text{new}}} \quad (6)$$

$$= T_t^{R \rightarrow O^{\text{new}}} T_t^{O \rightarrow M} \quad (7)$$

$$= T_t^{R \rightarrow O^{\text{new}}} (T_t^{R \rightarrow O})^{-1} T_t^{R \rightarrow M} \quad (8)$$

To compute $T_t^{R \rightarrow O^{\text{new}}}$ for $t > 0$, we assume the object follows the same relative motion as in the demonstration, but starting from the new initial pose. This can be computed as:

$$T_t^{R \rightarrow O^{\text{new}}} = T_1^{R \rightarrow O^{\text{new}}} (T_1^{R \rightarrow O})^{-1} T_t^{R \rightarrow O} \quad (9)$$

Substituting this into our equation for the new middle-finger trajectory:

$$T_t^{R \rightarrow M^{\text{new}}} = T_1^{R \rightarrow O^{\text{new}}} (T_1^{R \rightarrow O})^{-1} T_t^{R \rightarrow O} (T_t^{R \rightarrow O})^{-1} T_t^{R \rightarrow M} \quad (10)$$

$$= T_1^{R \rightarrow O^{\text{new}}} (T_1^{R \rightarrow O})^{-1} T_t^{R \rightarrow M} \quad (11)$$

This simplifies to:

$$T_t^{R \rightarrow M^{\text{new}}} = T_{\text{RELATIVE}} T_t^{R \rightarrow M} \quad (12)$$

where $T_{\text{RELATIVE}} = T_1^{R \rightarrow O^{\text{new}}} (T_1^{R \rightarrow O})^{-1} = T_1^{R \rightarrow O} T_1^{O \rightarrow O^{\text{new}}} (T_1^{R \rightarrow O})^{-1}$ is the transformation that accounts for the change in the initial object pose. This transformation is applied to the entire middle-finger trajectory, effectively adjusting the demonstration to the new initial object pose while preserving the relative motion between the object and the middle-finger.

To execute object-aware replay in the real world, we can directly track this new joint trajectory with joint PD control.

4) *Behavior Cloning Details:* To train a Diffusion Policy, we need to collect a dataset of observation and action pairs. Because we only have one human demonstration, we can generate additional demonstration data by introducing small amounts of transformation noise to the object’s pose and then use the process above to compute robot joint configuration trajectories with adjusted IK targets that account for this noise. Specifically, we sample $T_1^{O \rightarrow O^{\text{new}}}$ with the same translation and rotation noise as used in RL training and then run the object-aware replay computation above to get new object pose trajectories and robot joint configuration trajectories. The observation consists of the vector of robot joints q_t , the palm pose p_t^{palm} , and the object pose p_t^{object} . The action consists of joint position targets relative to the current robot position. We train with batch size of 128, 50 diffusion iterations, learning rate of $1e-4$, and a weight decay of $1e-6$. We use the state-based diffusion policy implementation from Drolet et al. [15].